

# Model Predictive Control for Vehicle Yaw Stability with Practical Concerns

Mooryong Choi and Seibum B. Choi, *Member, IEEE*

**Abstract**—This paper presents a method for ESC based on model predictive control (MPC) using the bicycle model with lagged tire force to reflect the lagged characteristics of lateral tire forces on the prediction model of the MPC problem for the better description of the vehicle behaviour. In order to avoid the computational burden in finding the optimal solution of the MPC problem using the constrained optimal control theory, the desired states and inputs as references are generated since the solution of the MPC problem can be obtained easily in a closed form without using numeric solvers using these reference values. The suggested method controls the vehicle to follow the generated reference values to maintain the vehicle yaw stability while the vehicle turns as the driver intended. The superiority of the proposed method is verified through comparisons with an ESC method based on ordinary MPC in the simulation environments on both high- $\mu$  and low- $\mu$  surfaces using the vehicle dynamics software CarSim.

**Index Terms**—Electronic stability control (ESC), model predictive control (MPC), vehicle dynamics, vehicle yaw stability.

## NOMENCLATURE

$C_x$	Tire longitudinal stiffness parameter
$C_\alpha$	Tire lateral stiffness parameter
$C_f$	Lumped cornering stiffness of front tires
$C_r$	Lumped cornering stiffness of rear tires
$\mu$	Tire-road friction coefficient
$F_z$	Tire normal force
$F_x$	Tire longitudinal force
$F_{yf}$	Front axle lateral tire force
$F_{yr}$	Rear axle lateral tire force
$\delta_f$	Average front steer angle
$r$	Vehicle yaw rate
$\beta$	Vehicle side slip angle
$l_f$	CG-front axle distance
$l_r$	CG-rear axle distance
$I_z$	Vehicle yaw moment of inertia
$m$	Vehicle mass
$v_x$	Vehicle longitudinal speed
$v_y$	Vehicle lateral speed
$R_e$	Tire effective radius
$M_z$	Corrective yaw moment
$N$	Prediction horizon
$P_B$	Brake cylinder pressure of each wheel
$t$	Vehicle half track

## I. INTRODUCTION

The authors are with the Department of Mechanical Engineering, KAIST (Korea Advanced Institute of Science and Technology), Daejeon 305-701, Korea (e-mail: mucho@kaist.ac.kr; sbchoi@kaist.ac.kr).

**T**O COPE with the increased demand for vehicle safety, various vehicle dynamic control systems have been introduced in the market over the past two decades [1]–[13]. Among these systems, the electronic stability control (ESC) systems, which stabilize the vehicle yaw motion by actuating the differential braking, have proved themselves to be one of the most effective systems for enhancing vehicle safety [14]. Although numerous types of ESCs have been developed by many researchers [15], [16], these ESC algorithms are most commonly activated to exert the corrective yaw moment to the vehicle when excessive differences in the actual and desired yaw rates or immoderate side slip angles are detected. However, when excessive side slip angles or excessive differences in the actual and desired yaw rates are observed, in many cases, the vehicle has already entered an unstable vehicle state. Since a vehicle in an unstable state tends to rapidly spin or bounce out of its desired trajectory, even a short delay in ESC actuation can result in fatal accidents. In order to overcome this drawback of the conventional ESCs, several papers in the literature [17]–[20] have suggested the methods that stabilize the yaw motion of a vehicle based on the model predictive control (MPC) scheme, which can predict the near future using vehicle dynamics models, so that early activations of the corrective yaw moments to stabilize the vehicle, even when the vehicle is in a stable vehicle state, are enabled to prevent the vehicle from entering an unstable state.

Although, the performances of the algorithms in [17]–[20] are reasonably satisfactory, according to the experimental or simulation results, several issues that must be considered for the MPC-based yaw stability control algorithms are not taken into account in these papers. First, the vehicle prediction models in MPC must reflect the lagged characteristics of tire forces. The majority of researches applying MPC to vehicle yaw stability rely on a bicycle model which is a simplified two-state vehicle dynamics model in predicting the future behavior of a vehicle. However, the bicycle model does not describe the lagged characteristics of lateral tire forces. Since the prediction time of the MPC formulation for vehicle yaw stability control is typically 0.1–0.3 s [17], [20] while the time constant for the lagged dynamics of lateral tire force can be up to 0.15 s, the prediction model for MPC for vehicle yaw stability control must reflect the lagged characteristics of the tire forces. Second, the MPC-based yaw stability control algorithms cause a significant computational burden in finding the optimal solutions of the MPC formulations which is the biggest obstacle that prevents MPC-based vehicle yaw stability control algorithms from being applied to commercial vehicles. This computational burden primarily originates

from the nonlinearities of the vehicle models and inequality constraints to restrain the state of the vehicle model within certain bounds in the MPC problem. Considering these issues, in this manuscript, the bicycle model with lagged tire forces is developed for use in the prediction model of MPC to reflect the lagged characteristics of tire forces for better description of the vehicle behavior. The nonlinear characteristics of tire forces, such as the friction ellipse effect or the tire force saturation, are taken into account by linearizing the tire forces about their operating points in order to reduce the computational burden when processing the complicated nonlinear tire model. In order to remove the inequality constraints for the state of the bicycle model, the MPC is designed to control the vehicle to follow the desired states instead of restraining them using inequality constraints. This paper is organized as follows: The overall structure of the MPC-based ESC algorithm is illustrated in Section II. The vehicle models used for the MPC formulation are introduced in Section III. The method of generating desired states and inputs is developed in Section IV. In Section V, the supervisory controller that generates the required corrective yaw moment to control the vehicle is presented with the MPC formulation and its closed form solution. In Section VI, the coordinator that minimizes the required absolute values of the brake forces to recreate the corrective yaw moment from the supervisor to apply to the vehicle is developed. The suggested algorithm is analyzed and verified using the vehicle dynamics software CarSim in Section VII. Concluding remarks are given in Section VIII.

## II. CONTROL ARCHITECTURE

In this section, the control structure and its intrinsic modular structure used to stabilize the vehicle lateral dynamics are presented. Figure 1 illustrates the main controller that consists of the supervisor and coordinator, the required sensor signals, and the estimators. Utilizing the readily available sensor signals in commercial vehicles including  $\delta_f$ , wheel speeds ( $\omega_i$ ), engine torque ( $T_e$ ), brake pressures ( $P_{b,i}$ ), longitudinal acceleration ( $a_x$ ), lateral acceleration ( $a_y$ ), and  $r$ , the estimators calculate the values of  $v_x$ ,  $v_y$ ,  $F_{x,i}$ ,  $F_{yf}$ ,  $F_{yr}$ , and  $F_{z,i}$  where  $i = 1, 2, 3, 4$  which correspond to the left-front, right-front, left-rear, and right-rear wheels, respectively. The estimated values are sent to the tire parameter identifier and the supervisor. In the tire parameter identifier, the values of  $C_x$ ,  $C_\alpha$ , and  $\mu$  are estimated using the estimated vehicle speeds and tire forces using the linearized recursive least squares method. The supervisor collects the information about the vehicle state and tire parameters and then generates the  $M_z$  to be exerted on the vehicle. After receiving  $M_z$  from the supervisor, the coordinator calculates the minimum required  $P_{b,i}$  to recreate  $M_z$  and apply it to each wheel. The estimator for  $v_x$  and  $v_y$  is based on the combination of a bicycle model and a kinematic model which is a multiple-observer system that computes the weighted sum estimation. The estimator for  $C_x$ ,  $C_\alpha$ , and  $\mu$  utilize the linearized recursive least squares method to identify these values in real time. For more details about the used estimators and the tire parameter identifier, refer to [21] and [22], respectively.

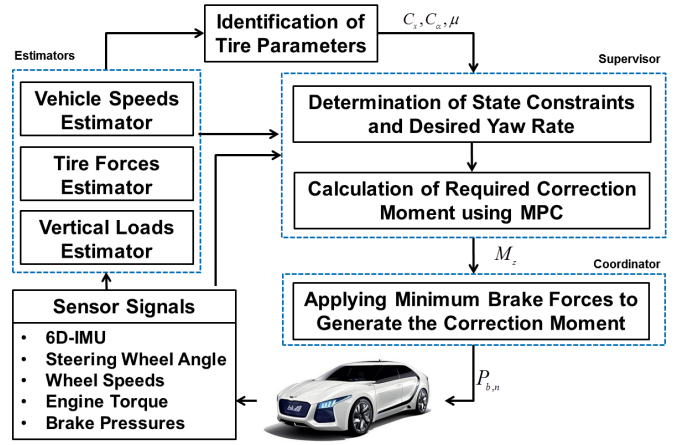


Fig. 1. Architecture of the ESC based on MPC

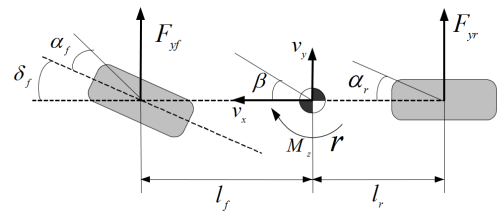


Fig. 2. Schematic of vehicle lateral dynamic model.

## III. VEHICLE MODELS

To operate the supervisor with the MPC scheme, two linear vehicle models are required: the linear bicycle model to generate the desired yaw rate and the bicycle model based on linearized tire forces to predict the future vehicle behavior. These two vehicle models that are integrated with the dynamic tire model [23] are developed to take the lagged characteristics of the tire forces into account.

### A. Bicycle Model with Lagged Tire Forces

The bicycle model is a dynamic model based on the vehicle lateral dynamics as shown in Fig. 2. The equations of motion for the vehicle lateral dynamics are as follows:

$$mv_x(\dot{\beta} + r) = F_{yf} + F_{yr}, \quad (1)$$

$$I_z \dot{r} = l_f F_{yf} - l_r F_{yr} + M_z, \quad (2)$$

where the lateral front and rear tire forces are simplified with the linear tire models as follows:

$$F_{yf} = C_f \alpha_f, \quad (3)$$

$$F_{yr} = C_r \alpha_r, \quad (4)$$

where

$$\alpha_f = \delta_f - \left( \beta + \frac{l_f \cdot r}{v_x} \right), \quad (5)$$

$$\alpha_r = -\beta + \frac{l_r \cdot r}{v_x}. \quad (6)$$

In (5) and (6),  $\alpha_f$  and  $\alpha_r$  are the slip angles of the front and rear tires, respectively.  $v_x$  is assumed to be constant for a short period time.

The dynamic tire model developed in [23] can be described as follows:

$$\tau_{lag} \dot{F}_{yf\_lag} + F_{yf\_lag} = F_{yf}, \quad (7)$$

$$\tau_{lag} \dot{F}_{yr\_lag} + F_{yr\_lag} = F_{yr}, \quad (8)$$

where  $F_{yf\_lag}$  and  $F_{yr\_lag}$  are the lagged lateral tire force of the front and rear tires, respectively.  $\tau_{lag}$  is the relaxation time constant defined as:

$$\tau_{lag} = \frac{C_\alpha}{K_e v_x} \quad (9)$$

where  $K_e$  is the equivalent tire lateral stiffness. Using the lagged tire forces (7) and (8), (1) and (2) can be rewritten as follows:

$$mv_x(\dot{\beta} + r) = F_{yf\_lag} + F_{yr\_lag}, \quad (10)$$

$$I_z \dot{r} = l_f F_{yf\_lag} - l_r F_{yr\_lag} + M_z. \quad (11)$$

By augmenting (7)-(11), a vehicle model including the dynamic tire model can be obtained in a state-space form as follows:

$$\dot{x} = Ax + B_\delta \delta_f + B_M M_z, \quad (12)$$

where

$$x = [\beta \quad \dot{\beta} \quad r \quad \dot{r}]^T \quad (13)$$

$$A = \begin{bmatrix} 0 & 1 & 0 & 0 \\ -\frac{C_f + C_r}{\tau_{lag} m v_x} & -\frac{1}{\tau_{lag}} & \left( \frac{C_r l_r - C_f l_f}{\tau_{lag} m v_x^2} - \frac{1}{\tau_{lag}} \right) & -1 \\ 0 & 0 & 0 & 1 \\ \frac{C_r l_r - C_f l_f}{\tau_{lag} I_z} & 0 & -\frac{C_f l_f^2 + C_r l_r^2}{\tau_{lag} I_z v_x} & -\frac{1}{\tau_{lag}} \end{bmatrix},$$

$$B_\delta = \begin{bmatrix} 0 \\ \frac{C_f}{\tau_{lag} m v_x} \\ 0 \\ \frac{C_f l_f}{\tau_{lag} I_z} \end{bmatrix} \quad B_M = \begin{bmatrix} 0 \\ 0 \\ 0 \\ \frac{1}{\tau_{lag} I_z} \end{bmatrix}.$$

### B. Tire Model

The bicycle model with the lagged tire forces in (12) can accurately describe the vehicle lateral motion only when the lateral tire forces exhibit linear characteristics as expressed in (3) and (4). However, ESCs are often activated when the generated tire forces exhibit the nonlinear characteristics, such as the friction ellipse effect or the tire force saturation, since vehicles tend to be unstable when the generated tire forces are close to their frictional limits. Therefore, the following longitudinal and lateral combined brushed tire model [23], [24] that can adequately describe the tires' nonlinear characteristics was adopted in the design of the supervisor controller.

$$F_{x,i} = \frac{C_x \left( \frac{\kappa_i}{1 + \kappa_i} \right)}{f_i} F_i, \quad (14)$$

$$F_{y,i} = -\frac{C_\alpha \left( \frac{\tan \alpha_i}{1 + \kappa_i} \right)}{f_i} F_i, \quad (15)$$

where

$$F_i = \begin{cases} f_i - \frac{1}{3\mu F_{z,i}} f_i^2 + \frac{1}{27\mu^2 F_{z,i}^2} f_i^3 & \text{if } f_i \leq 3\mu F_{z,i} \\ \mu F_{z,i} & \text{else} \end{cases}$$

$$f_i = \sqrt{C_x^2 \left( \frac{\kappa_i}{1 + \kappa_i} \right)^2 + C_\alpha^2 \left( \frac{\tan \alpha_i}{1 + \kappa_i} \right)^2}$$

$$\kappa_i = \frac{r_{e,i} \omega_i - v_{xt,i}}{v_{xt,i}}, \quad (16)$$

$$\begin{bmatrix} \alpha_1 \\ \alpha_2 \\ \alpha_3 \\ \alpha_4 \end{bmatrix} = \begin{bmatrix} \delta_f \\ \delta_f \\ 0 \\ 0 \end{bmatrix} - \tan^{-1} \begin{bmatrix} \frac{v_y + l_{fr}}{v_x} \\ \frac{v_y + l_{fr}}{v_x} \\ \frac{v_x - l_{rr}}{v_y} \\ \frac{v_x - l_{rr}}{v_y} \end{bmatrix}. \quad (17)$$

In (14) and (15),  $\kappa_i$  and  $\alpha_i$  denote the slip ratio and slip angle of  $i$ th wheel as defined in (16) and (17) respectively,  $\omega_i$  is the wheel speed, and  $v_{t,i}$  is the speed of the vehicle at the tire position. In [22], the plots of the interactions of  $F_x$ 's and  $F_y$ 's along with  $\alpha$ 's at different fixed  $\kappa$ 's and  $\mu$ 's with constant  $F_z$ 's using (14) and (15) are presented.

### C. Bicycle Model with Linearized Tire Forces

Using the method presented in [22], the values of  $C_x$ ,  $C_\alpha$ , and  $\mu$  are identified and updated at every time step to reflect the change in the surface conditions and the nonlinear characteristics of the tires in operating the suggested controller. Once these values are determined, it is possible to plot a lateral tire force curve along with  $\alpha$  by maintaining the other variables, such as  $F_z$  and  $\kappa$ , constants. By differentiating the lateral tire force curves with respect to the current  $\alpha$ ,  $C_{f0}$ , and  $C_{r0}$  can be obtained. Using  $C_{f0}$  or  $C_{r0}$  and the current operating points, the first degree polynomials of the  $\alpha$ 's are expressed as follows:

$$F_{yf} = C_{f0} \alpha_f + F_{yf0}, \quad (18)$$

$$F_{yr} = C_{r0} \alpha_r + F_{yr0}. \quad (19)$$

In (18) and (19),  $C_{f0}$  and  $C_{r0}$  represent the local slopes of the lateral tire force curves at the current  $\alpha$ 's while  $F_{yf0}$  and  $F_{yr0}$  indicate the residual tire forces that are  $F_y$ -intercepts of the first degree polynomials as shown in Fig. 3b. Since the shapes of the tire force curves from the tire model (14) and (15) vary depending on the values of not only the tire parameters but also  $F_z$  and  $\kappa$  as shown in [22], the nonlinear characteristics of the tire forces such as the tire force saturation and friction ellipse effect are taken into account by locally linearizing the lateral tire force curve at the currently operating point.

Instead of (3) and (4), (18) and (19) are substituted into (7) and (8). Due to the additional terms,  $F_{yf0}$  and  $F_{r0}$  in (18) and (19), the extra term,  $E_{add}$  is created in the following linear vehicle model in a state-space form:

$$\dot{x} = Ax + B_\delta \delta_f + B_M M_z + E_{add}, \quad (20)$$

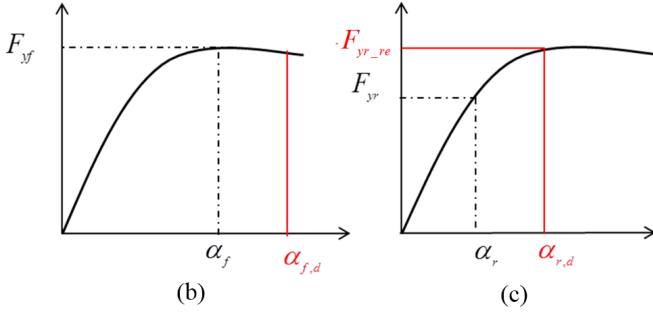
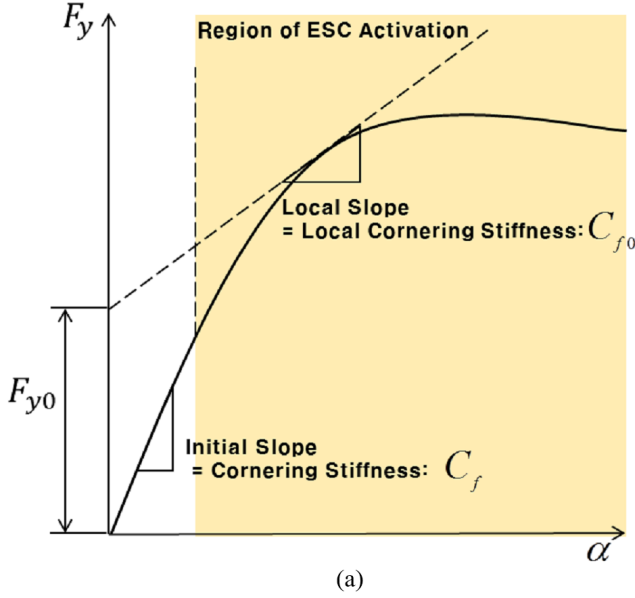


Fig. 3. Lateral tire forces: (a) Linearization for vehicle modeling. (b) Front axle of Understeering vehicle. (c) Rear axle of Understeering vehicle.

where

$$A = \begin{bmatrix} 0 & 1 & 0 & 0 \\ -\frac{C_{f0}+C_{r0}}{\tau_{lag}mv_x} & -\frac{1}{\tau_{lag}} & \left( \frac{C_{r0}l_r - C_{f0}l_f}{\tau_{lag}mv_x^2} - \frac{1}{\tau_{lag}} \right) & -1 \\ 0 & 0 & 0 & 1 \\ \frac{C_{r0}l_r - C_{f0}l_f}{\tau_{lag}I_z} & 0 & -\frac{C_{f0}l_f^2 + C_{r0}l_r^2}{\tau_{lag}I_z v_x} & -\frac{1}{\tau_{lag}} \end{bmatrix}$$

$$B_{\delta} = \begin{bmatrix} 0 \\ \frac{C_{f0}}{\tau_{lag}mv_x} \\ 0 \\ \frac{C_{f0}l_f}{\tau_{lag}I_z} \end{bmatrix} \quad B_M = \begin{bmatrix} 0 \\ 0 \\ 0 \\ \frac{1}{\tau_{lag}I_z} \end{bmatrix} \quad E_{add} = \begin{bmatrix} 0 \\ \frac{F_{0f}+F_{0r}}{\tau_{lag}mv_x} \\ 0 \\ \frac{l_f F_{0f} - l_r F_{0r}}{\tau_{lag}I_z} \end{bmatrix}$$

#### IV. GENERATION OF DESIRED STATES AND INPUTS

##### A. Generation of Desired Yaw Rates

In order to control the vehicle as the driver intended, the desired yaw rates that can be references for the vehicle to follow are required. The  $N$  number of desired yaw rates are generated using the bicycle model (12) by holding the current driver's steering input and the longitudinal velocity for the prediction time. However, since the bicycle model (12) does

not reflect the frictional limits of the tire forces, the absolute values of the desired yaw rates need to be truncated using appropriate upper bounds. The absolute values of the desired yaw rates have to satisfy the following inequality condition:

$$|r_{d,n}| \leq \left| \frac{(F_{yf\_max} + F_{yr\_max})}{mv_x} \right|, \quad (21)$$

where  $r_{d,n}$  denotes the desired yaw rate at the  $n$ th time step;  $F_{yf\_max}$  and  $F_{yr\_max}$  represent the maximum lateral front and rear axle forces, respectively.  $F_{yf\_max}$  and  $F_{yr\_max}$  can be obtained using the tire model (14) and (15). Since  $F_{yf\_max}$  and  $F_{yr\_max}$  vary along with  $\mu$  and  $\kappa_i$ ,  $r_{d,n}$  can be adequately constrained based on the surface condition and the friction ellipse effect.

##### B. Generation of Desired Side Slip Angles

The majority of ESCs is activated to restrain excessive  $\beta$  of a vehicle in a passive manner. Typically, ESCs are initiated to restrict  $\beta$  when its value exceeds approximately  $5^\circ$  [16]. However, to make full use of the tire forces to their frictional limits while turning, an appropriate value of  $\beta$  is required to generate the lateral tire forces to turn the vehicle as the driver intended since  $\alpha_i$ 's are functions of several variables including  $\beta$ . When the ESCs work to merely decrease the value of  $\beta$  when an immoderate  $\beta$  is detected, significant deteriorations of overall performances of ESCs are expected.

In order to avoid this problem, in this paper, the suggested ESC algorithm is designed to control the vehicle to track not only  $r_d$  but also the desired side slip angle,  $\beta_d$  to reflect the driver's intention on the control of the vehicle, while maintaining the stability of the vehicle in a turn. To illustrate the procedure of generating  $\beta_d$ , a vehicle in an understeered turn is taken as an example.

When a vehicle understeers, since the front lateral tire forces saturate first, an additional  $\alpha_f$  followed by a larger  $\delta_f$  from the driver does not provide any larger lateral tire forces than  $F_{yf\_max}$ . Consequently, at this state that is represented by the dotted line in Fig. 3b, the absolute value of the yaw rate does not increase since no additional corrective yaw moment, which is a function of the additional lateral tire force, is created along with the increasing steering input. However,  $F_{yr}$  is not yet fully saturated as shown in Fig. 3c with the dotted line. Since the sum of the front and rear lateral tire forces have to be equal to the centrifugal force that is exerted on the turning vehicle in the steady state with given  $r$  and  $v_x$ , the maximum  $r$  of the turning vehicle at a given  $v_x$  can increase by enlarging the value of the unsaturated  $F_{yr}$ . The unsaturated  $F_{yr}$  can increase as the absolute value of  $\alpha_r$ , which is a function of  $\beta$ , grows. Accordingly, the value of the desired side slip angle,  $\beta_d$  is determined to increase  $F_{yr}$  to  $F_{yr\_re}$  which is defined as follows:

$$F_{yr\_re} = mv_x r_d - F_{yf\_max}, \quad (22)$$

where  $mv_x r_d$  is assumed to be the centrifugal force that is exerted on the vehicle in a turn with  $r_d$  and  $v_x$ .

Using the tire model (14) and (15), the desired rear tire slip angle,  $\alpha_{r,d}$  which corresponds with  $F_{yr\_re}$  can be obtained.  $\beta_d$  can be easily acquired rearranging (6) with the given  $F_{yr\_re}$ .

Because both  $\alpha_f$  and  $\alpha_r$  grow simultaneously along with an increasing  $\beta$  as expressed in (5) and (6),  $\alpha_f$  also moves to the front desired tire slip angle,  $\alpha_{f,d}$  indicated by the solid red lines in Fig. 3(b). The corrective yaw moment to be exerted on the vehicle is calculated to track  $\beta_d$  and  $r_d$ . As  $N$  number of  $r_d$  are calculated in the previous subsection,  $N$  number of  $\beta_d$  are also generated. To obtain  $\beta_d$ , when a vehicle oversteers, (22) can be replaced by the following equation:

$$F_{yf\_re} = mv_x r_d - F_{yr\_max}. \quad (23)$$

After then, the same procedure to obtain  $\beta_d$  when the vehicle understeers can be carried out by switching  $\alpha_{r,d}$  to  $\alpha_{f,d}$ .

### C. Generation of Desired Corrective Yaw Moment

In the procedure of determining  $\beta_d$ , although  $F_{y*re}$  is obtained to balance the centrifugal force and the lateral tire forces, the moment balance of the vehicle in a steady state turn is not maintained. In order to secure the moment balance of the vehicle, by letting  $\dot{r} = 0$  in (2), the desired corrective yaw moment,  $M_{z\_d}$  is acquired as follows:

$$\begin{aligned} \text{Understeering: } M_{z\_d} &= -l_f F_{yf} + l_r F_{yr\_re}, \\ \text{Oversteering: } M_{z\_d} &= -l_f F_{yf\_re} + l_r F_{yr}. \end{aligned}$$

## V. MPC FOR SUPERVISOR

In the previous sections, the bicycle models and the desired states for the vehicle to follow are suggested. In this section, the MPC scheme that can provide the optimal corrective yaw moment to be applied to the vehicle to track the desired state is described.

### A. MPC Formulation

A model predictive controller finds a set of optimal inputs, that minimize the cost function while satisfying the input constraints over a specified prediction time horizon and it applies only the first input in the sequence of the optimal inputs to the system at each time step. First, in order to form an MPC problem, the bicycle model with linearized tire forces (20) was discretized using zero-order hold as follows:

$$x_{k+1} = A_k x_k + B_{M,k} u_k + E_k, \quad (24)$$

where

$$E_k = B_{\delta,k} \delta_f + E_{add,k}, \quad u_k = M_{z,k}.$$

The subscript  $k$  denotes that the corresponding discretized matrices are at the  $k$ th step in discrete time. The terms in  $E_k$ , including  $\delta_f$ , are set to be constants while developing (24) for the prediction time span. The cost function of MPC with equality constraints in quadratic form is defined as follows:

$$J(x(0), U) = \sum_{k=0}^{N-1} (x_k - x_{d,k})' Q (x_k - x_{d,k}) \cdots \quad (25)$$

$$\begin{aligned} &+ (u_k - u_{d,k})' R (u_k - u_{d,k}) + (x_N - x_{N,k})' P (x_N - x_{N,k}) \\ \text{subj. to } &x_{k+1} = A_k x_k + B_{M,k} u_k + E_k, \quad (26) \end{aligned}$$

where

$$U = [u_0, \dots, u_{N-1}]'$$

with  $Q$ ,  $P$ , and  $R$  which are the weighting matrices with corresponding dimensions.  $x_d$  and  $u_d$  refer to the desired state and corrective yaw moment, respectively.

### B. Closed Form Solution for MPC

Since the bicycle model (12) with the linearized tire model is linear and the inequality constraints in the quadratic cost function (25) are omitted, the closed form solution of the MPC problem can be acquired without using numerical solvers when the MPC controller is designed for the vehicle to follow the desired states with the desired inputs. The terms with constant values, which do not affect the value of the optimal solution, can be removed from (25) and it can be rewritten as follows:

$$J(x(0), U) = \sum_{k=0}^{N-1} x_k' Q x_k - 2x_{d,k}' Q x_k \cdots \quad (27)$$

$$+ u_k' R u_k - 2u_{d,k}' R u_k + x_N' P x_N - 2x_{d,N}' P x_N.$$

The equality constraints in (26) can be explicitly rewritten with all future states,  $x_1, x_2, \dots, x_N$  and the future inputs,  $u_0, u_1, \dots, u_{N-1}$ :

$$\begin{aligned} \underbrace{\begin{bmatrix} x(0) \\ x_1 \\ \vdots \\ x_N \end{bmatrix}}_X &= \underbrace{\begin{bmatrix} I \\ A_{l,k} \\ \vdots \\ A_{l,k}^N \end{bmatrix}}_{S^x} x(0) \cdots \\ &+ \underbrace{\begin{bmatrix} 0 & \cdots & \cdots & 0 \\ B_{B,k} & 0 & \cdots & 0 \\ A_{l,k} B_{B,k} & \ddots & \ddots & \vdots \\ \vdots & \ddots & \ddots & \vdots \\ A_{l,k}^{N-1} B_{B,k} & \cdots & \cdots & B_{B,k} \end{bmatrix}}_{S^u} \underbrace{\begin{bmatrix} u_0 \\ \vdots \\ \vdots \\ u_{N-1} \end{bmatrix}}_U \quad (28) \\ &\cdots + \underbrace{\begin{bmatrix} 0 \\ E_k \\ A_{l,k} E_k + E_k \\ \vdots \\ A_{l,k}^{N-1} E_k + \cdots + E_k \end{bmatrix}}_{S^e} \end{aligned}$$

Since all future states are explicit functions of the present state ( $x(0)$ ) and the future and current inputs ( $u_0, u_1, \dots, u_{N-1}$ ), (28) can be expressed as follows in a compact form:

$$X = S^x x(0) + S^u U + S^e. \quad (29)$$

Using  $X$  as shown in (28), the cost function (27) can be rewritten as follows:

$$J(x(0), U) = X' \bar{Q} X + U' \bar{R} U + T X + T_u, \quad (30)$$

where

$$\begin{aligned} \bar{R} &= \text{blockdiag}\{R, \dots, R\}, \\ \bar{Q} &= \text{blockdiag}\{Q, \dots, Q, P\}, \\ T &= -2X_d' \bar{Q}, \\ T_u &= -2U_d' \bar{R}, \end{aligned}$$

with

$$\begin{aligned} X_d &= [x_{d,0}, \dots, x_{d,N}]', \\ U_d &= [u_{d,0}, \dots, u_{d,N-1}]', \end{aligned}$$

By substituting (29) into (30), the cost function (30) can be rewritten as follows:

$$J(x(0), U) = (S^x x(0) + S^u U + S^e)' \bar{Q} (S^x x(0) + S^u U + S^e) \cdots + U' \bar{R} U + T (S^x x(0) + S^u U + S^e) + T_u. \quad (31)$$

By dropping the terms with constant values and rearranging, the cost function (31) can be modified:

$$J(x(0), U) = U' (S^{u'} \bar{Q} S^u + \bar{R}) U \cdots + [2x'(0)(S^{x'} \bar{Q} S^u) + 2S^{e'} \bar{Q} S^u + T S^u + T_u] U \quad (32)$$

Since (32) has the form of a positive definite quadratic function, its minimum can easily be obtained by differentiating (32) with respect to  $U$  and finding  $U^*$  that sets it to zero. The optimal inputs  $U^*$  with the given desired states are obtained:

$$U^*(x(0), T, T_u) = -\frac{1}{2} (S^{u'} \bar{Q} S^u + \bar{R})^{-1} [2x'(0)(S^{x'} \bar{Q} S^u) \cdots + 2S^{e'} \bar{Q} S^u + T S^u + T_u]'. \quad (33)$$

The MPC scheme finds the optimal solution ( $U^*$ ) at each time step. However, only the current step input is utilized and the remaining future inputs are discarded. The corrective yaw moment is applied to the vehicle by allocating differential brake forces to the wheels. The method of allocating differential brake forces for the given corrective yaw moment is introduced in the next section.

## VI. COORDINATOR FOR OPTIMAL DISTRIBUTION OF BRAKE FORCES

The supervisor controller presented in the previous section generates the corrective yaw moment ( $M_z$ ), to stabilize the vehicle at each time step. The corrective yaw moment can be exerted on the vehicle by applying the differential brake forces. In this section, the coordinator that determines the minimum required brake forces and which wheel should apply the brake forces is developed. Fig. 4 shows the examples of two different cases exerting positive yaw moments on the vehicle in a right turn by applying brake forces on the front left wheel and rear left wheel. When applying a brake force on the front left wheel as seen in Fig. 4a, the lateral force decreases along with an increased longitudinal force due to the friction ellipse effect seen in [22]. The decreased lateral force multiplied by  $\sin \delta_f \cdot l_f$  is added to the resultant corrective yaw moment. In contrast, when applying the brake force on the rear left wheel, the decreased lateral force multiplied by  $l_r$  due to the increased longitudinal force is subtracted from the resultant corrective yaw moment as shown in Fig. 4b. The plots of the amounts of the resultant corrective yaw moments along with increasing slip ratios of the front and the rear wheels are presented in Fig. 4. The values of the corrective yaw moments can be expressed as follows:

$$M_{zf} = \sin \delta_f \cdot l_f \cdot \Delta F_{yf} + \cos \delta_f \cdot t \cdot \Delta F_{xf}, \quad (34)$$

$$M_{zr} = t \cdot \Delta F_{xr} - l_r \cdot \Delta F_{yr}, \quad (35)$$

where  $M_{zf}$  and  $M_{zr}$  denote the corrective yaw moments applied by the front and rear wheels respectively.  $\Delta F_{x*}$  and  $\Delta F_{y*}$  are

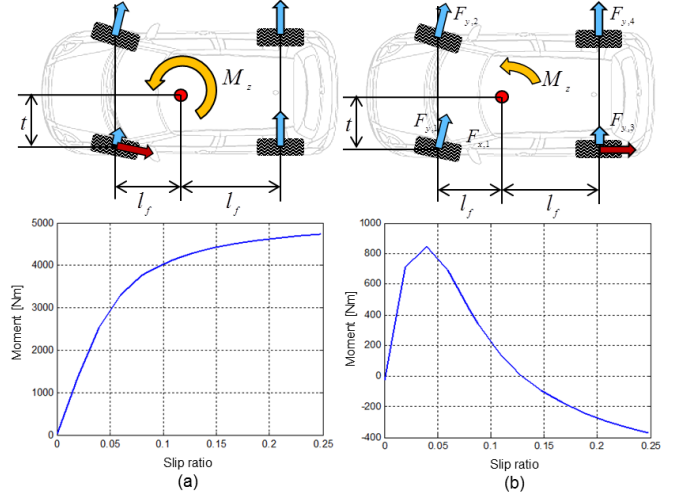


Fig. 4. Comparison of the resultant corrective yaw moment when applying brake forces: (a) on the front left wheel and (b) on the rear left wheel.

the amounts of changes in the longitudinal force and lateral force, respectively, caused by applying brake forces on the front or rear wheel, respectively.  $\Delta F_{y*}$  at the given  $\alpha_i$  with the varying  $\kappa_i$  can be obtained using the tire model (14) and (15). To optimally distribute the brake forces, the following cost function is defined:

$$J_M(\Delta F_{xf}, \Delta F_{xr}) = |\Delta F_{xf}| + |\Delta F_{xr}|, \quad (36)$$

$$\text{subj. to } M_z = M_{zf} + M_{zr}. \quad (37)$$

Newton-Raphson method finds the optimal solution ( $\Delta F_{xf}^*$  and  $\Delta F_{xr}^*$ ) that minimizes the cost function ( $J_M$ ) in (36) while satisfying the equality constraint (37) at every time step. The values of brake pressure that can generate  $\Delta F_{xf}^*$  and  $\Delta F_{xr}^*$  at a given state are calculated using the following equations:

$$P_{B*} = \frac{\Delta F_{x*}}{K_{B*}}, \quad (38)$$

where  $P_{B*}$  and  $K_{B*}$  denote the required cylinder brake pressure and brake gain of the corresponding wheel, respectively.

## VII. SIMULATION RESULTS AND DISCUSSION

The performance of the proposed MPC-based ESC algorithm was evaluated by simulations using the D-class sedan model in the CarSim software. In order to verify its effectiveness, the suggested algorithm was compared with a conventional ESC algorithm based on an ordinary MPC in the simulation environments with low- $\mu$  and high- $\mu$  surfaces. The ordinary MPC based on the typical bicycle model (1) and (2), which do not consider lagged tire force dynamics, was formulated for the conventional algorithm to follow the reference yaw rates without constraints for the side slip angle. Furthermore, simulations using only lagged tire forces or  $\beta_d$  were also performed to independently verify their effectiveness. The values of the parameters for the simulation are presented in Table I.  $t_s$  is the size of the time step for running the controller.  $t_p$  is the size of the time step for the prediction model (24). The prediction time can be  $t_p \cdot N$ .

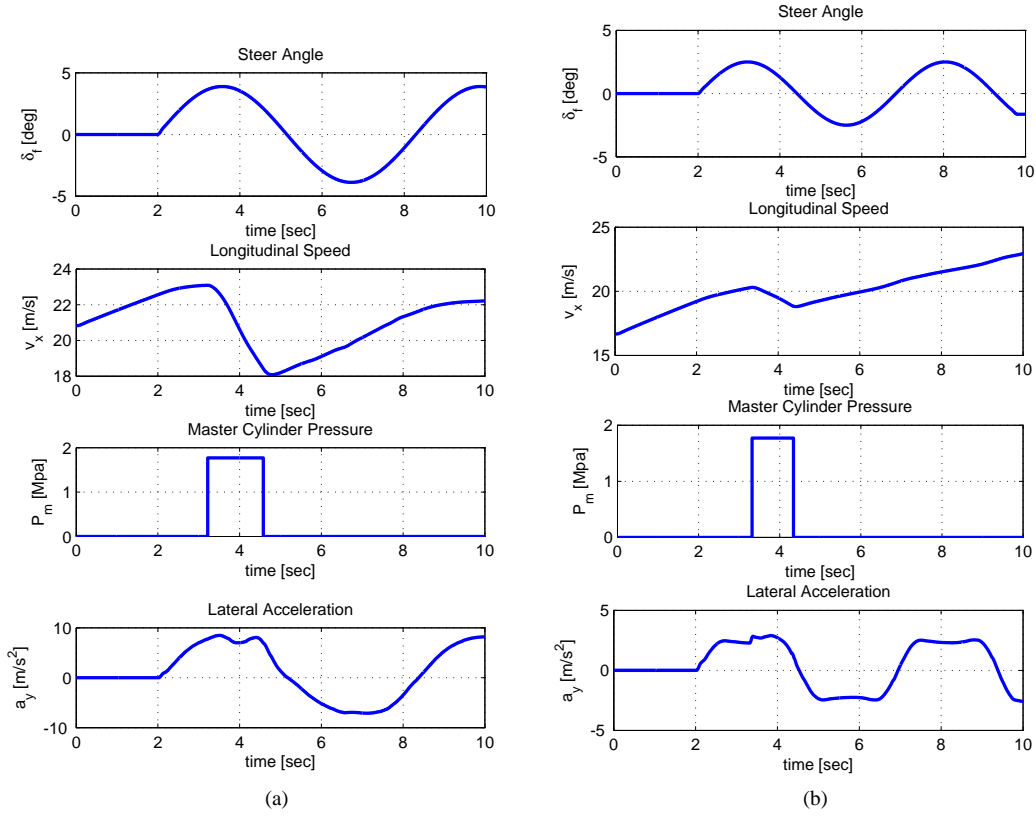


Fig. 5. Vehicle maneuvers: (a) On a high- $\mu$  surface ( $\mu = 0.85$ ) (b) On a low- $\mu$  surface ( $\mu = 0.3$ ).

TABLE I  
PARAMETERS FOR SIMULATION

Parameter	Value	Parameter	Value
$N$	8	$Q$	$\text{diag}\{1, 0, 7, 0\} \cdot 10^9$
$t_s$ [sec]	0.02	$R$	1
$t_p$ [sec]	0.03	$P$	$\text{diag}\{1, 0, 7, 0\} \cdot 10^9$

### A. Simulation on a High- $\mu$ Surface

In the first simulation whose maneuvers and results are presented in Fig. 5a and Fig. 6a, respectively, the verification of the suggested MPC-based ESC algorithm was carried out in the simulation environment on a high- $\mu$  surface with  $\mu = 0.85$ . The brake was applied by the driver at approximately  $t = 4$  s during turning to spin the vehicle out to recreate a harsh simulation scenario. As shown in Fig. 6a, since the brake was applied when the vehicle was at the limit of handling, the vehicle spins out when no control action was taken. The conventional ESC algorithm based on ordinary MPC could keep the vehicle from bouncing out from  $r_d$ . However, the immoderate deviation of  $r$  from  $r_d$  was detected compared with that of the suggested algorithm. Despite the values of the integrations of  $M_z'$ s over the simulation time, which correspond to the lost kinetic energy during the brake actuation of the vehicle, for the conventional and suggested methods being almost identical, the value of  $\beta$  for the conventional method was significantly larger compared with that of the suggested method since early actuation of the differential braking was

enabled with the suggested method to track  $\beta_d$ .

In order to validate the effectiveness of the suggested method on a low- $\mu$  surface, a simulation with the maneuver shown in Fig. 5b was performed on a low- $\mu$  surface with  $\mu = 0.3$ . As in the first simulation on a high- $\mu$  surface, the brake was applied at approximately  $t = 4$  s during the slalom maneuvering. As shown in Fig. 6b, when any control action was not taken by the ESC system, the vehicle understeered and an excessive  $\beta$  was observed. Although the understeer is corrected using the conventional method, still the deviation of  $r$  from  $r_d$  is detected with the excessive  $\beta$ . In contrast, the suggested method minimized the deviation of  $r$  from  $r_d$  while maintaining the value of  $\beta$  near the value of  $\beta_d$ . The better performance of the suggested method was achieved even with the smaller absolute value of  $M_z$ .

### B. Analysis of the Effectiveness of Applying $\beta_d$ or Lagged Tire Forces

The previous simulations were performed by applying both  $\beta_d$  and lagged tire forces to demonstrate the superiority of the suggested algorithm by maximizing the performance of the MPC controller. In this subsection, two simulations were conducted on a high- $\mu$  surface. The first simulation was conducted with the bicycle model reflecting the lagged tire forces but without  $\beta_d$ . In contrast, the controller in the second simulation was set to follow  $\beta_d$  without including the lagged tire forces in the bicycle model. The vehicle maneuvers and results of the first simulation are presented in Fig. 7a and

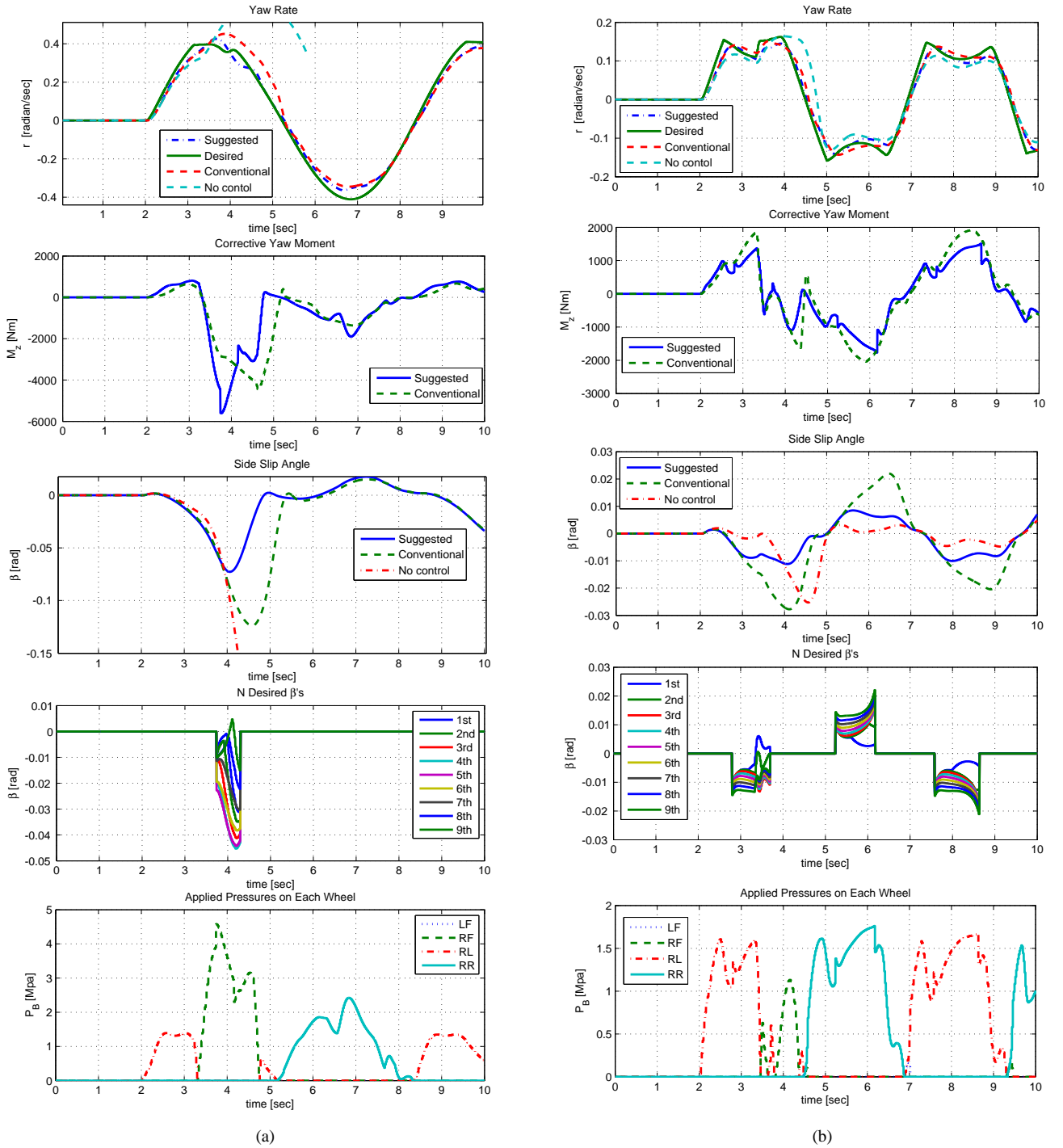


Fig. 6. Simulation results: (a) On a high- $\mu$  surface ( $\mu = 0.85$ ) (b) On a low- $\mu$  surface ( $\mu = 0.3$ ).

Fig. 7c, respectively. As shown in Fig. 7c, thanks to the more accurate prediction of the vehicle behavior from the bicycle model including the lagged tire forces, the earlier actuation could be enabled. As a result, when applying the lagged tire force in the prediction model, the MPC controller could stabilize the vehicle with a smaller value of the maximum corrective yaw moment. It was also verified that applying an adequate corrective yaw moment at a proper time to follow  $r_d$  reduces the maximum value of  $\beta$  during the vehicle maneuver.

In the second simulation, whose maneuvers and results are presented in Fig. 7b and Fig. 7d, respectively, it was proven that setting the MPC controller to follow not only  $r_d$  but also  $\beta_d$  is advantageous in stabilizing the vehicle lateral motion. Even without reflecting the lagged tire forces in the prediction model of the MPC controller, tracking  $\beta_d$  to generate appropriate lateral tire forces is beneficial in controlling the vehicle to follow  $r_d$ . At the same time, the maximum value of  $\beta$  during the vehicle maneuver was also minimized compared with when

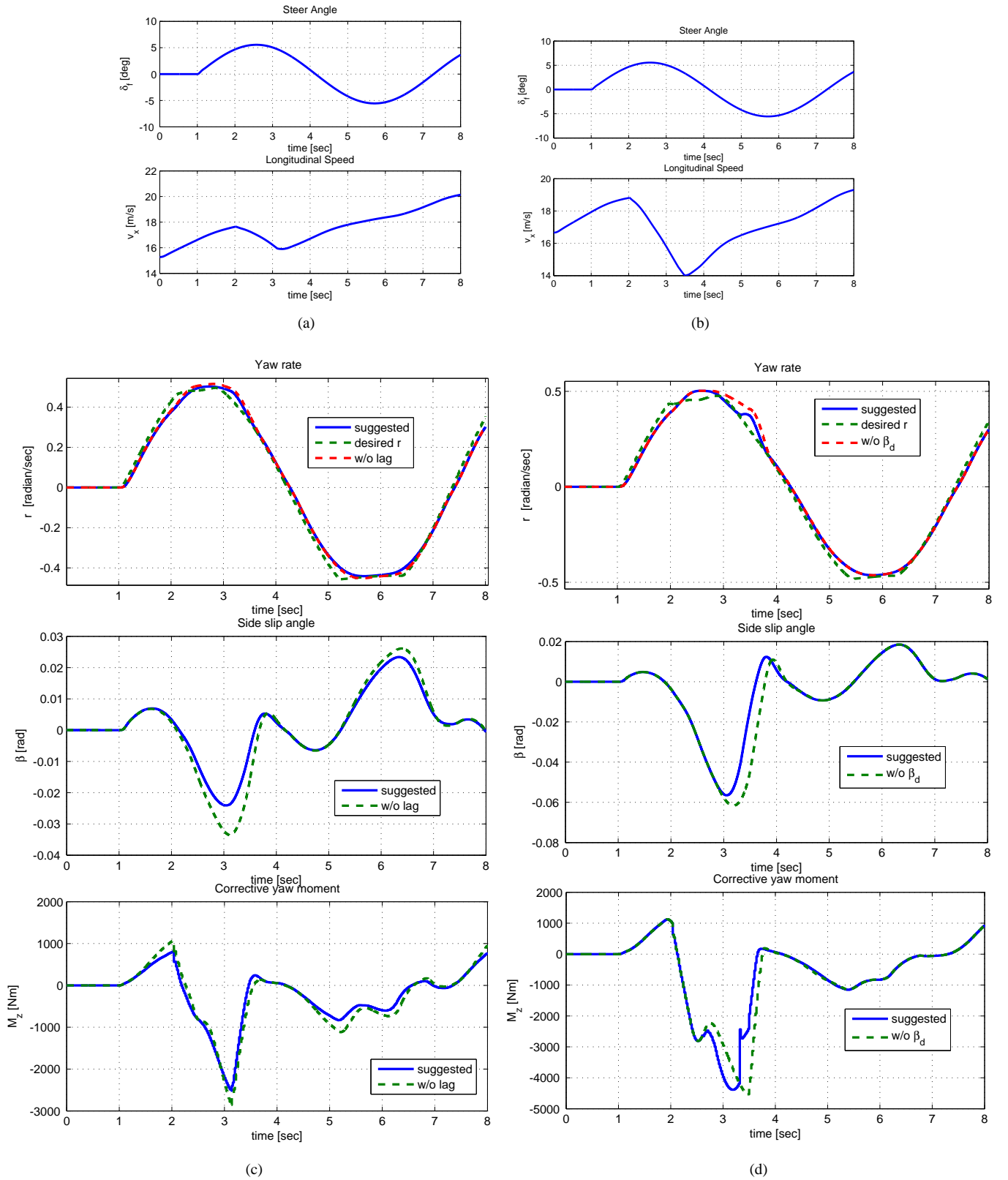


Fig. 7. Simulation analysis: (a) Maneuver for verification of reflecting lags of tire forces. (b) Maneuver for verification of tracking  $\beta_d$ . (c) Comparison of with and without reflecting the lags of tire forces. (d) Comparison of with and without tracking  $\beta_d$ .

the case that  $\beta_d$  was not applied. Furthermore, when applying  $\beta_d$ , the maximum value of the corrective yaw moment applied to the vehicle was slightly smaller.

## VIII. CONCLUSION

A novel method of ESC based on MPC was developed and investigated in the CarSim simulation environment. The

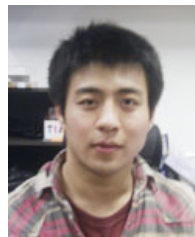
proposed algorithm distinguishes itself from the previously reported methods by the following features: (1) it can reflect the lagged characteristics of lateral tire forces on the prediction model in the MPC formulation to better predict vehicle behavior; (2) it generates the desired values of side slip angle and corrective yaw moment to maintain the vehicle yaw stability while driving the vehicle as the driver intended; (3) a closed form solution for the MPC problem with the desired state and inputs was obtained without requiring iterations of numeric solvers; (4) it optimally allocates the brake forces considering the friction ellipse effect with the current vehicle state and vertical loads. The simulation results of the suggested MPC-based ESC demonstrate that the suggested method can control the vehicle to track the desired states with minimum control inputs both on a high- $\mu$  and low- $\mu$  surfaces.

#### ACKNOWLEDGEMENT

This work was supported by the National Research Foundation of Korea (NRF) grant funded by the Korea government Ministry of Science, ICT & Future Planning (MSIP), (No. 2010-0028680) and the MSIP, Korea, under the C-ITRC (Convergence Information Technology Research Center) support program (NIPA-2013-H0401-13-1008) supervised by the NIPA (National IT Industry Promotion Agency)

#### REFERENCES

- [1] C. Ahn, B. Kim, and M. Lee, "Modeling and control of an anti-lock brake and steering system for cooperative control on split- $\mu$  surfaces," *Int. J. Automot. Technol.*, vol. 13, no. 4, pp. 571–581, 2012.
- [2] K. Nam, H. Fujimoto, and Y. Hori, "Robust yaw stability control for electric vehicles based on active front steering control through a steer-by-wire system," *Int. J. Automot. Technol.*, vol. 13, no. 7, pp. 1169–1176, 2012.
- [3] M. H. Lee, K. S. Lee, H. G. Park, Y. C. Cha, D. J. Kim, B. Kim, S. Hong, and H. H. Chun, "Lateral controller design for an unmanned vehicle via kalman filtering," *Int. J. Automot. Technol.*, vol. 13, no. 5, pp. 801–807, 2012.
- [4] W. Z. Zhao, Y. J. Li, C. Y. Wang, Z. Q. Zhang, and C. L. Xu, "Research on control strategy for differential steering system based on h mixed sensitivity," *Int. J. Automot. Technol.*, vol. 14, no. 6, pp. 913–919, 2013.
- [5] J. Takahashi, M. Yamakado, and S. Saito, "Evaluation of preview g-vectoring control to decelerate a vehicle prior to entry into a curve," *Int. J. Automot. Technol.*, vol. 14, no. 6, pp. 921–926, 2013.
- [6] J. Song, "Integrated control of brake pressure and rear-wheel steering to improve lateral stability with fuzzy logic," *Int. J. Automot. Technol.*, vol. 13, no. 4, pp. 563–570, 2012.
- [7] R. Tchamna and I. Youn, "yaw rate and side-slip control considering vehicle longitudinal dynamics," *Int. J. Automot. Technol.*, vol. 14, no. 1, pp. 53–60, 2013.
- [8] M. H. Lee, K. S. Lee, H. G. Park, Y. C. Cha, D. J. Kim, B. Kim, S. Hong, and H. H. Chun, "Lateral controller design for an unmanned vehicle via kalman filtering," *Int. J. Automot. Technol.*, vol. 13, no. 5, pp. 801–807, 2012.
- [9] B. Song, "Cooperative lateral vehicle control for autonomous valet parking," *Int. J. Automot. Technol.*, vol. 14, no. 4, pp. 633–640, 2013.
- [10] S. Manso and M. A. Passmore, "Effect of rear slant angle on vehicle crosswind stability simulation on a simplified car model," *Int. J. Automot. Technol.*, vol. 14, no. 5, pp. 701–706, 2013.
- [11] X. Wang and L. J. S. Shi, L. Liu, "Analysis of driving mode effect on vehicle stability," *Int. J. Automot. Technol.*, vol. 14, no. 3, pp. 363–373, 2013.
- [12] Y. S. Zhao, W. N. Bao, I. P. Chen, and Y. Q. Zhang, "Fuzzy adaptive sliding mode controller for an air spring active suspension," *Int. J. Automot. Technol.*, vol. 13, no. 7, pp. 1057–1065, 2013.
- [13] S. H. Jeong, J. E. Lee, S. U. Choi, and K. H. L. J. N. Oh, "Technology analysis and low-cost design of automotive radar for adaptive cruise control system," *Int. J. Automot. Technol.*, vol. 13, no. 7, pp. 363–373, 2013.
- [14] J. Dang, "Preliminary results analyzing the effectiveness of electronic stability control (esc) systems," tech. Rep. DOT-HS-809-790, U.S. Department of Transportation, Washington, DC, 2004.
- [15] D. Kim, K. Kim, W. Lee, and I. Hwang, "Development of mando esp (electronic stability program)," in *SAE 2003 Wor. Cong. and Exh.*, no. 2003-01-0101, 2003.
- [16] A. T. van Zanten, R. Erthadt, and G. Pfaff, "Vdc, the vehicle dynamics control of bosch," in *SAE 1995 Int. Cong. and Expo.*, no. SAE950759, 1995.
- [17] G. Palmieri, O. Barbarisi, S. Scala, and L. Glielmo, "A preliminary study to integrate ltv-mpc lateral vehicle dynamics control with a slip control," in *Proc. 48th IEEE Conf. Decision and Control*, Shanghai, China, 2009, pp. 4625–4630.
- [18] D. Bernardini, S. D. Cairano, A. Bemporad, and H. Tseng, "Drive by-wire vehicle stabilization and yaw regulation: A hybrid model predictive control design," in *Proc. 48th IEEE Conf. Decision and Control*, Shanghai, China, 2009, p. 76217626.
- [19] C. E. Beal and J. C. Gerdes, "Model predictive control for vehicle stabilization at the limits of handling," *IEEE Trans. Contr. Syst. Technol.*, 2012, doi:10.1109/TCST.2012.2200826.
- [20] P. Falcone, F. Borrelli, J. Asgari, H. E. Tseng, and D. Hrovat, "Predictive active steering control for autonomous vehicle systems," *IEEE Trans. Contr. Syst. Technol.*, vol. 15, no. 3, pp. 566 – 580, 2007.
- [21] J. Oh and S. Choi, "Vehicle velocity observer design using 6d imu and multiple observer approach," *IEEE Trans. Intell. Transport. Syst.*, vol. 13, no. 4, pp. 1865–1879, 2012.
- [22] M. Choi, J. Oh, and S. B. Choi, "Linearized recursive least square methods for real-time identification of tire-road friction coefficient," *IEEE Trans. Veh. Technol.*, vol. 62, no. 7, pp. 2906 – 2918, 2013.
- [23] H. B. Pacejka, *Tire and Vehicle Dynamics*, 2nd ed. SAE, 2006.
- [24] Y. Hsu, "Applications of," Ph.D. dissertation, Stanford Univ., Stanford, CA, 2009.



**Mooryong Choi** obtained his B.S. degree in mechanical engineering from Yonsei University, Seoul, Korea in 2008 and the M.S. degree in mechanical engineering from University of California, Los Angeles, in 2010. He is currently a Ph.D. candidate of mechanical engineering from Korea Advanced Institute of Science and Technology (KAIST). His research interests include vehicle dynamics, control and computer vision.



**Seibum B. Choi** received B.S. degree in mechanical engineering from Seoul National University, Korea, M.S. degree in mechanical engineering from Korea Advanced Institute of Science and Technology (KAIST), Korea, and the Ph.D. degree in controls from the University of California, Berkeley in 1993. From 1993 to 1997, he had worked on the development of Automated Vehicle Control Systems at the Institute of Transportation Studies at the University of California, Berkeley. Through 2006, he was with TRW, MI, where he worked on the development of advanced vehicle control systems. Since 2006, he has been with the faculty of the Mechanical Engineering department at KAIST. His research interests include fuel saving technology, vehicle dynamics and control, and active safety systems.